

Experienced Deep Reinforcement Learning with Generative Adversarial Networks (GANs) for Model-Free Ultra Reliable Low Latency Communication

Ali Taleb Zadeh Kasgari *Student Member, IEEE*, Walid Saad, *Fellow, IEEE*,
Mohammad Mozaffari *Member, IEEE*, and H. Vincent Poor, *Fellow, IEEE*

Abstract

In this paper, a novel *experienced* deep reinforcement learning (deep-RL) framework is proposed to provide model-free resource allocation for ultra reliable low latency communication (URLLC) in the downlink of a wireless network. The proposed, experienced deep-RL framework can guarantee high end-to-end reliability and low end-to-end latency, under explicit data rate constraints, for each wireless user without any models of or assumptions on the users' traffic. In particular, in order to enable the deep-RL framework to account for extreme network conditions and operate in highly reliable systems, a new approach based on generative adversarial networks (GANs) is proposed. This GAN approach is used to pre-train the deep-RL framework using a mix of real and synthetic data, thus creating an experienced deep-RL framework that has been exposed to a broad range of network conditions. Formally, the URLLC resource allocation problem is posed as a power minimization problem under reliability, latency, and rate constraints. To solve this problem using experienced deep-RL, first, the rate of each user is determined. Then, these rates are mapped to the resource block and power allocation vectors of the studied wireless system. Finally, the end-to-end reliability and latency of each user are used as feedback to the deep-RL framework. It is then shown that at the fixed-point of the deep-RL algorithm, the reliability and latency of the users are near-optimal. Moreover, for the proposed GAN approach, a theoretical limit for the generator output is analytically derived. Simulation results show how the proposed approach can achieve near-optimal performance within the rate-reliability-latency region, depending on the network and service requirements. The results also show that the proposed experienced deep-RL framework is able to remove the transient training time that makes conventional deep-RL methods unsuitable for URLLC. Moreover, during extreme conditions, it is shown that the proposed, experienced deep-RL

A. Taleb Zadeh Kasgari and W. Saad are with Wireless@VT, Department of ECE, Virginia Tech, Blacksburg, VA, 24060, USA. Emails: {alitek, walids}@vt.edu. M. Mozaffari is with Ericsson Research, Santa Clara, CA, 95054, USA, Email: mohammad.mozaffari@ericsson.com. H. V. Poor is with the Department of Electrical Engineering, Princeton University, Princeton, NJ, 08544, USA, Email: poor@princeton.edu.

A preliminary version of this work appeared in IEEE ICC, [1].

agent can recover instantly while a conventional deep-RL agent takes several epochs to adapt to new extreme conditions.

Index Terms—Resource allocation, Deep reinforcement learning, generative adversarial networks, low latency communications

I. INTRODUCTION

Ultra reliable low latency communication (URLLC) will be one of the most important features in next-generation 5G and beyond cellular networks as it will be necessary for mission critical applications such as Internet of Things (IoT) [2] sensing and control as well as remote control of autonomous vehicles and drones [3], [4]. Thus far, prior URLLC research has been mostly focused on applications that require low data rates such as uplink transmissions of IoT sensors [3], [5]. However, new wireless applications such as drone communications [2], autonomous driving [6], [7], and virtual reality [8], have emerged. These applications require URLLC, not only in the uplink, but also in the downlink for control, navigation, and tracking purposes. Moreover, in order to operate effectively, such applications require both URLLC and certain data rate guarantees. For example, autonomous vehicles will need to receive reliable control data from infrastructure, along with high data rate information such as HD maps. Similarly, virtual reality applications will use URLLC for tracking users, but will also require high data rates with high reliability for transmitting, in real-time, the virtual environment videos and images.

Providing URLLC with rate considerations for beyond 5G applications poses many network challenges. First, such applications are very sensitive to wireless network environment fluctuations and, therefore, they require wireless resource management solutions that are reliable in face of *extreme network conditions* (e.g., unexpected traffic patterns or worst-case randomness of the wireless channel). Second, considering the limited radio resources in a communication system, low latency, high reliability, and high rate can become three incompatible design parameters. This incompatibility means that improving one of them could potentially be detrimental to the other two, thus requiring *new designs that can be used to balance the rate-reliability-latency tradeoff* for the aforementioned applications [3]. Third, maintaining high reliability and low latency needs timely and efficient resource allocation. Hence, URLLC resource allocation with rate considerations should allocate the exact amount of resources required by the users. In other words, in order to provide URLLC links, the resource management system of a cellular system must be able to sustain extreme network conditions. Moreover, to balance the rate-reliability-latency

tradeoff, any resource allocation scheme must learn each user's exact performance requirements so that it can satisfy them without wasting any resources or reducing the user's reliability.

A. *Related Works*

Recently, there has been a surge in literature that studies problems of URLLC and resource allocation, such as in [3], [9]–[17]. In [9], the authors use extreme value theory to study URLLC in a vehicular network and characterize the queue statistics. The work in [10] considers a model-based and a data-driven approach for designing a burstiness-aware scheduling framework which reserves bandwidth for users with bursty traffic. The authors in [11] propose a packet prediction mechanism to predict the behavior of future incoming packets based on the packets in the current queue. In [12], the authors propose a hybrid resource allocation, to allocate dedicated resources and a shared resource pool to a set of wireless users with URLLC requirements considering channel and users' traffic conditions. Meanwhile, the work in [13] introduces a method for joint user association and resource allocation for URLLC heterogeneous networks. A joint transmit power and resource allocation for vehicular networks subject to ultra reliability and low latency constraints is proposed in [14]. The work in [15] proposes a quality-of-service-aware resource allocation framework for vehicular networks. In [17], an algorithm for joint scheduling of URLLC and broadband traffic in 5G cellular systems is proposed. In [16], we studied the problem of providing low latency communication for human-centric applications considering the reliability of human users. However, all of these existing works assume that explicit traffic and queue models are available to the resource allocation system [3], [9]–[17]. Since the assumed models are often simplified, they either underestimate or overestimate the users' traffic and queue lengths. This can cause the resource allocation algorithm to either allocate more resources or less resources than the actual requirement of the users which, in turn, can render the system inefficient or degrade the reliability of the users' connections. Moreover, prior works which consider extreme cases for URLLC [9] with a simplified traffic model, cannot handle practical extreme network scenarios which further motivates a model-free approach. Further, the previous works on URLLC completely ignore any rate requirements of the users and some of them such as [10] and [11] heavily rely on historical data which can also lead to inefficient resource allocation because a user's traffic often changes based on spatial or temporal factors. In fact, even if it is available, historical data is often not a precise predictor of the traffic of wireless users.

To overcome some of these challenges, there has been recent interest in using deep reinforcement learning (deep-RL) for solving wireless networking problems with incomplete information [6], [18]–[23]. In [6], a decentralized resource allocation framework for vehicle-to-vehicle communications is proposed based on deep-RL. The authors in [18] propose a deep-RL resource management approach for virtualized ad-hoc network. In [24] a deep-RL resource management system is proposed for caching in cloud radio access networks. A deep-RL based resource allocation scheme for mobile edge computing is studied in [20]. The work in [21] proposes a deep supervised learning approach to solve the sub-band and power allocation problem in multi-cell networks. In [22], the authors propose a learning-based approach for wireless resource management by modeling the input-output relationship of a resource optimization algorithm with neural network. However, these works do not investigate URLLC problems. Moreover, since these deep-RL works [19]–[21] limit their problem’s action space, use discretization to manage the size of the action space [6], or do not address the limitation of deep-RL when dealing with large action spaces, they are not suitable for realistic URLLC resource management problems in actual wireless systems. This is because these works cannot handle the large action space involved in URLLC and they have high order of time complexity which makes them not suitable for the requirements of URLLC.

Collecting real data for training deep learning models is another challenge which is not properly addressed in the previous deep-RL works that mostly rely on simulated data [6], [18]–[23]. Although deep-RL methods do not need collecting data beforehand, a deep-RL agent can better perform if it is trained before being deployed. This is particularly needed for URLLC systems in which reliability is necessary. Indeed, even though deep-RL methods can collect data during the training process [25], as is true in the case of humans, a deep-RL agent can substantially enhance its prediction if it becomes more intelligent and experienced by exploiting more training datasets. Hence, if a deep-RL agent is deployed for URLLC purposes without training, it will initially be inexperienced at the beginning of the learning which can cause unreliability in the system. Most of the previous literature on deep-RL did not consider this issue of learning reliability [6], [18]–[21], [23] and hence are not easily applicable for URLLC applications. In a URLLC system, *intelligence and experience* are particularly important to enable the deep-RL agent to deal with *extreme and critical events* that occur in the wireless system and that can jeopardize the performance of the system. Examples of such extreme events include unusual traffic patterns, extremely scarce resource availability, unforeseen network congestion,

and deep fades that seldom occur, among others. In fact, the whole premise of URLLC is to provide reliability with respect to such extreme events [3], [9]–[11], [13]–[15], [17]. However, without gaining considerable experience through rigorous training, it becomes unlikely for deep-RL agents to frequently encounter such extreme events and, thus, they cannot cope with URLLC requirements. As a result, prior works on deep-RL [6], [18]–[23] that solely rely on online training may not be able to provide URLLC links at the level expected by 5G systems (i.e., very high reliability at very low latency). In order to overcome this unique URLLC challenge, we propose to develop an “*experienced*” *deep-RL agent* that can gain experience in a virtual environment before being deployed in an extremely reliable systems.

B. Contributions

The main contribution of this paper is a novel, model-free resource management framework that is reliable against extreme events and that can balance the tradeoff between reliability, latency, and data rate, without explicit prior assumptions on the system parameters such as the users’ traffic arrival model or the wireless environment. We formulate the problem as a model-free power minimization problem with reliability, latency, and rate considerations. To solve this problem, we propose a deep-RL framework that dynamically predicts the traffic model of the users and, then, uses those predictions to jointly allocate resource blocks (RBs) and power to downlink users, under URLLC and rate constraints. Then, we introduce a *generative adversarial network (GAN)-based refiner* to that can enable the proposed deep-RL agent to gain experience and learn extreme events. The proposed GAN-based refiner allows us to transform a limited set of real traffic and wireless channel data into a large dataset of realistic and diverse data that can be deployed for training the deep-RL agent and providing it with experience. Fig. 1 illustrates how we propose to use a virtual environment to increase the deep-RL agent’s experience. As we can see, the deep-RL agent will act in a virtual training environment and using virtual feedbacks it gains experience. Then, it is deployed in a real URLLC environment. The proposed framework is then shown to effectively find a near-optimal resource allocation solution such that the low latency, high reliability, and high rate requirements of the wireless users are satisfied. Also, it is shown that the GAN-generated dataset can enable the framework to gain experience in extreme events which allows it recover faster in the case of unpredicted rare events in a URLLC system.

In summary, our key contributions include:

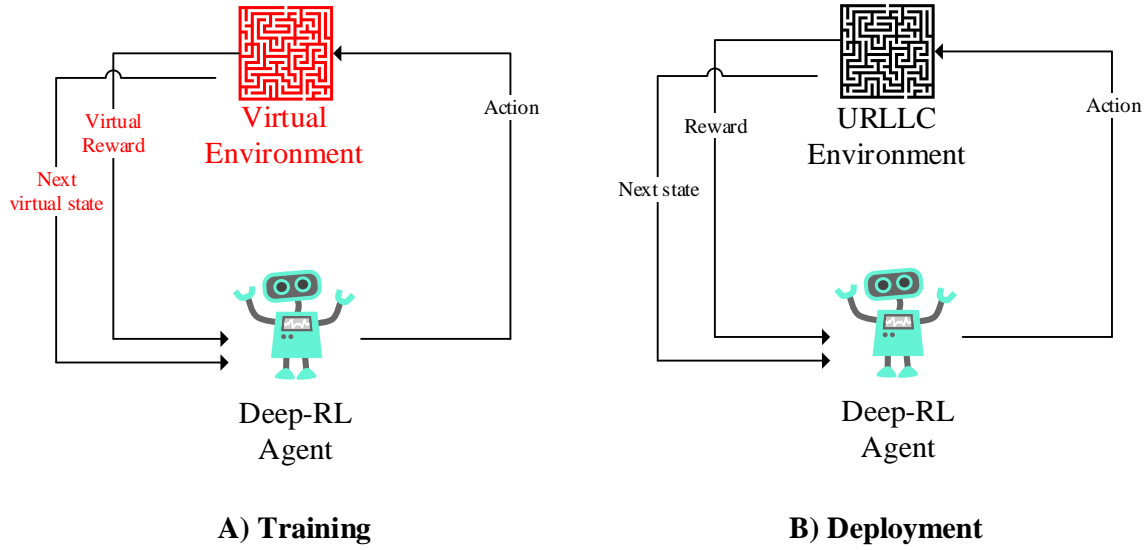


Figure 1: Providing deep-RL with network experience in a virtual environment before deployment in a real URLLC environment.

- The proposed deep-RL framework can dynamically measure the end-to-end reliability and the delay of each user. Then, it uses this measurement as online feedback to modify its decisions. In particular, the deep neural network (DNN) weights used in deep-RL are updated using this feedback only. Also, the proposed resource allocation system is then shown to be able to predict the consequences of its actions in the future and use this information to make better resource allocation decisions. This helps the algorithm provide long-term reliability and latency guarantees for the users.
- Unlike the deep-RL approaches that were previously used for wireless networks, e.g., in [6], [18]–[21], and [23], our approach does not rely on an inexperienced deep-RL agent in the system. In contrast, the proposed deep-RL framework is designed so as to gain network experience in a virtual environment generated by using the proposed GAN-based refiner. The use of GANs enables our deep-RL framework to avoid trial-and-errors imposed by other approaches. Hence, GAN makes the algorithm suitable for the use in URLLC scenarios. Creating this GAN-based virtual environment can also remove biases in the wireless datasets that stem from the fact that wireless channel information and packet arrival information are normally gathered in a specific time and location which makes them biased towards those spatio-temporal conditions.
- The proposed GAN model can use a real dataset with limited data points on the packet

arrival and wireless channel information to generate a comprehensive real dataset of packet arrival and channel information that can include extreme networking conditions. Then, the GAN-generated dataset, combined with the real dataset, can be fed into the deep-RL agent, to create an *experienced deep-RL agent* that can provide URLLC. To the best of our knowledge, none of the prior works in [6], [18]–[21], and [23], [25]–[28] developed an experienced deep-RL agent that makes use of GAN to learn extreme events and eliminate data set biases. We note that some works in wireless literature [29], [30], and [31] have used GAN. However, these works used GAN to solely identify the distribution of the wireless channel or for security purposes. Although our work identifies the channel and traffic distribution implicitly, it also gives the generator network the ability to generate extreme cases – an aspect that has not been investigated in any of previous works [29], [30]. We also analytically find a range for the generator network’s extreme cases.

- We enhance deep-RL scalability by addressing the large action space problem that stems from the fact that in the considered wireless network, there is a large set of actions which can be taken by deep-RL agent. This large set of actions makes the problem unsuitable for deep-RL frameworks [25]. In particular, we propose the novel concept of an *action space reducer* which reduces the size of the action space without limiting it. Using this action space reducer, our deep-RL framework can make decisions in real-time as opposed to discretization approach used in [6]. We show that when the proposed algorithm converges, the reliability, latency, and rate of each user are guaranteed.

Simulation results show that the proposed, experienced deep-RL framework can ensure reliability by eliminating the transient training time in the conventional deep-RL method. Moreover, during extreme conditions, our experienced deep-RL agent can recover almost instantly while it takes 50 epochs for a conventional deep-RL agent to adapt to new extreme conditions. This makes our proposed deep-RL agent more suitable for URLLC systems.

The rest of the paper is organized as follows. Section II introduces the system model. Sections III and IV, respectively, present the deep-RL and GAN-based virtual environment for model free URLLC. Section V presents the simulation results and conclusions are drawn in VI.

II. SYSTEM MODEL

Consider the downlink of an orthogonal frequency-division multiple access (OFDMA) cellular network with a single base station (BS) serving a set \mathcal{N} of N users and having a set \mathcal{K} of K

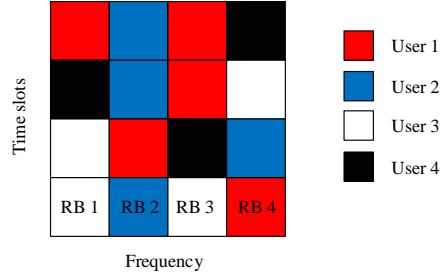


Figure 2: Resource block allocation for 4 different users in 4 time-slots.

available RBs. Each user has its own, individual rate, reliability, and latency requirements. We do not make any assumptions on the packet arrival or the packet length of each user. The downlink transmission rate from the BS to user i is:

$$r_i(t) = \sum_{j=1}^K \rho_{ij}(t) B \log_2 \left(1 + \frac{p_{ij}(t) h_{ij}(t)}{\sigma^2} \right), \quad (1)$$

where B is the RB bandwidth, and $h_{ij}(t)$ is the time-varying channel gain of the transmission from the BS to user i on RB j at time slot t . $p_{ij}(t)$ is the downlink transmission power of the BS on RB j to user i at slot t . $\rho_{ij}(t)$ is the RB allocation indicator with $\rho_{ij}(t) = 1$ when RB j is allocated to user i at time slot t , otherwise $\rho_{ij}(t) = 0$. $\sigma^2 = BN_0$ is the noise power with N_0 being the power spectral density of noise. An example of RB allocation for 4 users is shown in Fig. 2. The resource allocation system will decide on the composition of the users in each row (time slot).

We define *reliability* $\gamma_i(t)$ as the probability of the end-to-end instantaneous packet delay exceeding a predefined target end-to-end latency threshold D_i^{\max} for user i . This delay comprises the queuing delay, and the transmission delay. To satisfy the reliability and latency condition, the system needs to retain its rate so that it is larger than average arrival rate, i.e.,

$$r_i(t) > \phi(\lambda_i(t), \beta(t), \gamma_i, D_i^{\max}) > \lambda_i(t) \beta_i(t), \quad (2)$$

where $\beta_i(t)$ is the average packet size and $\lambda_i(t)$ is the average packet arrival rate of user i at time-slot t . Hence, $\lambda_i(t) \beta_i(t)$ captures the average arrival rate in bits per second (bps). ϕ is an unknown function that we will implicitly approximate using our proposed method. Our system's goal is to allocate resources to minimize the average downlink power while maintaining reliability, latency, and rate for the users. We now formally pose this resource allocation problem:

$$\min_{p_{ij}, \rho_{ij}} \lim_{t \rightarrow \infty} \frac{1}{t} \sum_{\tau=1}^t \sum_{i=1}^N \sum_{j=1}^K p_{ij}(\tau), \quad (3a)$$

$$\text{s.t } \Pr\{D_i > D_i^{\max}\} < 1 - \gamma_i^*, \quad \forall i \in \mathcal{N}, \quad (3b)$$

$$r_i(t) > \lambda_i(t)\beta_i(t), \quad \forall i \in \mathcal{N}, \quad \forall t \quad (3c)$$

$$p_{ij}(t) \geq 0, \quad \rho_{ij}(t) \in \{0, 1\},$$

$$\forall i \in \mathcal{N}, \quad \forall j \in \mathcal{K}, \quad \forall t, \quad (3d)$$

$$\sum_i \rho_{ij}(t) = 1, \quad \forall j \in \mathcal{K}, \quad \forall t. \quad (3e)$$

The objective function in (3a) is the average power spent by the BS. In (3b), D_i is the packet delay of user i . Constraint (3b) takes into account each user's reliability and latency explicitly. the rate constraint is considered both implicitly using (2) and explicitly in (3c). Constraint (3b) is a reliability condition that guarantees the end-to-end delay to be less than D_i^{\max} with a reliability of at least $1 - \gamma_i^*$. Constraints (3d) and (3e) are feasibility conditions.

At each time slot t , the resource allocation system has two functions: *Phase 1*: Determining the rate that each user i should obtain to ensure a target reliability γ_i^* and *Phase 2*: Allocating power and RBs to each user so that the power is minimized. Note that the minimum power in Phase 2 is a function of the data rates determined in Phase 1. To determine the reliability of the system in (3b), it is customary to use a specific queuing model, as done in all of the prior art [3], [9]–[17]. In contrast, to be model-free, we propose to obtain the reliability in (3b) using an empirical measurement of the number of packets transmitted to user i whose delay exceeds D_i^{\max} over the total number of packets transmitted (to user i) in time slot t , i.e.,

$$\gamma_i(t) = 1 - \Pr\{D_i > D_i^{\max}\} \approx 1 - \frac{\mu'_i(t)}{\mu_i(t)}, \quad (4)$$

where $\mu'_i(t)$ is the number of packets transmitted to user i in time slot t , whose end-to-end delay exceeds D_i^{\max} . $\mu_i(t)$ is the total number of packets transmitted to user i in time slot t . By doing so, we do not need to make any a priori assumptions on the delay model of the users. Moreover, counting the number of packets is a simple and practical feedback for the network, because each user can convey this information to the BS via a control channel. As $\mu_i(t)$ grows, the approximation converges to the reliability in (3b). As will be evident from Section V, despite having no model for the traffic, the proposed approach will still be able to ensure the target reliability and delay for each user. Table I provides a list of our main parameters and notations.

Since the OFDMA resource allocation problem involves a large state space and we have no prior knowledge of the traffic models, we propose a deep-RL framework [25] to allocate resources to the users so that their rate requirement and their stringent reliability constraints are

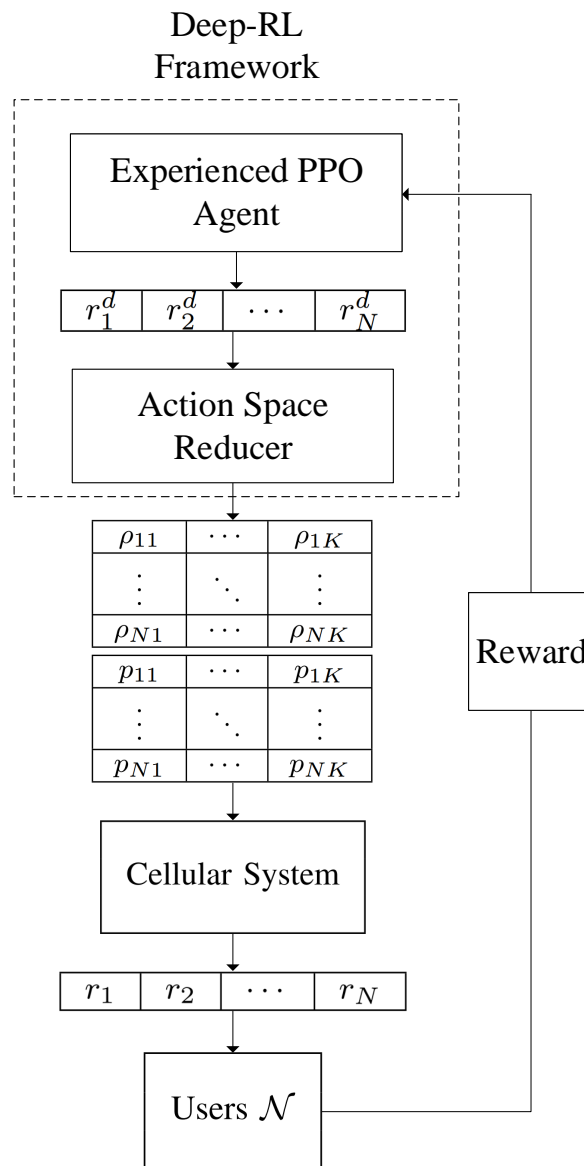


Figure 3: Block diagram for the proposed framework.

satisfied. Beyond being able to operate without any model, the key advantage of deep-RL over classical reinforcement learning (RL) is that it can solve control problems with a large state space [25]. Deep-RL uses a deep neural network approximating the action-value function in RL.

Similar to humans, gaining valuable experience on the network model can take a long time for a deep-RL agent because extreme network conditions or events will rarely occur in the system. Given that URLLC requires reliability to such extreme events, it is imperative the our deep-RL agent be equipped with enough experience on the system. In particular, if we can reproduce these situations for our deep-RL agent in a virtual environment, then it can gain experience rapidly

Table I: List of notations.

Notation	Description	Notation	Description
B	RB bandwidth	$\mathbf{a}_t, \mathcal{A}$	Action and action space
N	Number of users	\mathbf{s}, \mathcal{S}	State and state space
K	Number of available RBs	$\pi_\psi(\mathbf{a}_t \mathbf{s}_t)$	Policy function
$\mu_i(t)$	Total number of packets transmitted to user i in time slot t	A_t	Advantage function
$\mu'_i(t)$	Number of packets transmitted to user i in time slot t whose end-to-end delay exceeds D_i^{\max}	$F(\cdot; \theta_R)$	Refiner output
D_i	Packet delay for user i	z	Refiner input
$\beta_i(t)$	Average packet size for user i at time slot t	θ_D	Discriminator set of weights
$\lambda_i(t)$	Average packet arrival rate of user i at time slot t	θ_R	Refiner set of weights
$h_{ij}(t)$	Time-varying channel gain for user i on RB j	$D(\cdot; \theta_D)$	Discriminator output
$\rho_{ij}(t)$	RB allocation indicator for user i on RB j	\mathcal{N}	Set of users
$p_{ij}(t)$	Downlink transmission power for user i on RB j	\mathcal{K}	Set of RBs
$\gamma_i(t)$	Reliability for user i	r_i	User i actual rate
D_i^{\max}	Target end-to-end latency threshold for user i	r_i^d	User i desired rate
$w_i(t)$	Time-varying weight	N_0	Power spectral density of noise

and provide ultra reliability to the network. We propose to generate such an environment for our deep-RL agents by using a GAN-based refiner, as explained in Section IV.

III. DEEP-RL FOR MODEL FREE URLLC

The proposed deep-RL framework will use two feedback inputs to evaluate its performance and update its DNN in each time slot: The total BS downlink power in each time slot $P(t) = \sum_{i=1}^N \sum_{j=1}^K p_{ij}(t)$ and the measured reliability of each user at each time using (4). Using those two inputs, the deep-RL framework can determine $\rho_{ij}(t)$ and $p_{ij}(t)$ for all i and j . After iteratively assigning $\rho_{ij}(t)$ and $p_{ij}(t)$ and receiving the needed feedback in a few time slots, the system can maintain reliability, latency, and rate for each user.

Our deep-RL framework is shown in Fig. 3. From Fig 3, we can see that, at each time slot, the deep-RL algorithm will determine a desired rate $r_i^d(t)$ for each user i . Next, an action space reducer maps $r_i^d(t)$ to the OFDMA resources ρ_{ij} and p_{ij} for all $i \in \mathcal{N}$ and $j \in \mathcal{K}$ while minimizing the power (Section III-B). Then, each user attains the rate $r_i(t)$ (which is now close to $r_i^d(t)$) and finds a reward function (defined in (5)) and sends it as feedback to the deep-RL framework that uses this feedback and updates each user's $r_i^d(t)$ accordingly (Section III-C).

A. Deep-RL scheduling

We now formally define our deep-RL framework by determining its action-space \mathcal{A} , state-space \mathcal{S} , and reward function R . At each state $\mathbf{s}_t \in \mathcal{S}$, our deep-RL algorithm takes action $\mathbf{a}_t \in \mathcal{A}$ and receives a reward $R(\mathbf{a}_t, \mathbf{s}_t)$. For our wireless resource allocation problem, we consider the channel gains, the number of packets $\mu_i(t)$ transmitted to each user, and the average packet length $\beta_i(t)$ for each user i as the *state* $\mathbf{s}_t = (\mu_i(t), \beta_i(t), h_{ij}(t)), \forall i \in \mathcal{N}, j \in \mathcal{K}$, for the proposed deep-RL framework. The *action* $\mathbf{a}_t = (p_{ij}(t), \rho_{ij}(t)), \forall i, j$ is essentially the power and

RB allocation for any user i and for any RB j . Then, we determine the reward for deep-RL to guarantee URLLC without the delay model. Deep-RL will use this reward for training its DNN and approximating the action-value function. We define the reward for the proposed deep-RL framework as a function of power and reliability. However, it is implicitly a function of the state and action of the deep-RL algorithm. We define the reward as follows:

$$R(\mathbf{a}_t, \mathbf{s}_t) = - \sum_{i \in \mathcal{N}} w_i(t)(1 - \gamma_i(\mathbf{a}_t, \mathbf{s}_t)) - \alpha P(\mathbf{a}_t), \quad (5)$$

where α is a weighting factor for power and $P(\mathbf{a}_t) = \sum_{i=1}^N \sum_{j=1}^K p_{ij}(t)$. For notational simplicity, hereinafter, we use $\gamma_i(t)$ and $P(t)$ instead of $\gamma_i(\mathbf{a}_t, \mathbf{s}_t)$ and $P(\mathbf{a}_t)$. $w_i(t)$ is given by:

$$w_i(t+1) = \max\{w_i(t) + \gamma_i^* - \gamma_i(t), 0\}. \quad (6)$$

$w_i(t)$ is a time-varying weight that increases if $\gamma_i(t) < \gamma_i^*$. Hence, it ensures that the system meets the target reliability of the users. Next, we show that, when the proposed deep RL algorithm maximizes the reward in (5), the reliability and delay in (3b) are guaranteed for each user.

Theorem 1. If the BS maximizes the reward in (5), then after the convergence of the deep-RL algorithm, the reliability of each user is guaranteed such that $\gamma_i(t) \geq \gamma_i^* \forall i \in \mathcal{N}$.

Proof: First, assume that the value that $w_i(t)$ converges to is w_i^* . Then, we have to show:

$$\begin{aligned} \|w_i(t+1) - w_i^*\|^2 &= \|\max\{w_i(t) + \gamma_i^* - \gamma_i(t), 0\} - w_i^*\|^2 = \\ \|w_i(t) + \gamma_i^* - \gamma_i(t)\|^2 + \|w_i^*\|^2 - 2w_i^{*T}(w_i(t) + \gamma_i^* - \gamma_i(t)) &= \\ \|w_i(t) - w_i^*\|^2 + \|\gamma_i^* - \gamma_i(t)\|^2 - 2(w_i^* - w_i(t))^T(\gamma_i^* - \gamma_i(t)), \end{aligned}$$

Hence,

$$\begin{aligned} \|w_i(t+1) - w_i^*\|^2 - \|w_i(t) - w_i^*\|^2 &= \\ \|\gamma_i^* - \gamma_i(t)\|^2 - 2(w_i^* - w_i(t))^T(\gamma_i^* - \gamma_i(t)). \end{aligned} \quad (7)$$

Hence, if $\|\gamma_i^* - \gamma_i(t)\|^2 < 2(w_i^* - w_i(t))^T(\gamma_i^* - \gamma_i(t))$, The algorithm converges to its fixed point.

At the fixed-point of the algorithm, we know that $w_i(t+1) = w_i(t)$, therefore

$$w_i(t) + \gamma_i^* - \gamma_i(t) \leq \max\{w_i(t) + \gamma_i^* - \gamma_i(t), 0\} = w_i(t), \quad (8)$$

Thus, we can see that $w_i(t) + \gamma_i^* - \gamma_i(t) \leq w_i(t)$ and hence, $\gamma_i(t) \geq \gamma_i^*$. ■

Theorem 1 finds the condition for convergence of the algorithm, and ensures that the reliability of each user is guaranteed at the fixed-point of the algorithm, i.e., when $w_i(t) = w_i(t+1)$. Also,

the latency for each user is implicitly guaranteed by Theorem 1. The original action space for the deep-RL resource allocation problem is the possible set for ρ_{ij} and p_{ij} for all i and j which has the size of $\mathcal{O}(K^N) \times \mathbb{R}^K$. Therefore, in our URLLC problem, we have a large state space and a large action space. Even though deep-RL effectively addresses the large state space problem, we still have to address the large action space problem. To this end, next, we propose a novel mechanism, called *action space reducer*, using which we reduce the size of the action space. Such an approach to reduce the action space has not been done in prior deep-RL works [6] and [18]–[23].

B. Reducing Action Space by Optimal Power Allocation

The action space for the studied wireless resource allocation problem consists of the following $N \times K$ RB allocation matrix and $N \times K$ power allocation matrix:

$$\boldsymbol{\rho} = \begin{bmatrix} \rho_{11} & \cdots & \rho_{1K} \\ \vdots & \ddots & \vdots \\ \rho_{N1} & \cdots & \rho_{NK} \end{bmatrix}, \quad \mathbf{P} = \begin{bmatrix} p_{11} & \cdots & p_{1K} \\ \vdots & \ddots & \vdots \\ p_{N1} & \cdots & p_{NK} \end{bmatrix}.$$

Our mixed-integer action space size is $\mathcal{O}(K^N) \times \mathbb{R}^K$, and it is infeasible to search for the optimal action in such a space. This, in turn, can significantly slow down the convergence of deep-RL algorithms which hinders their applicability for any wireless resource management system. To address this problem, we propose an action space reducer framework that can reduce the size of action space to \mathbb{R}^N . This action space reducer essentially, converts the actions taken in \mathbb{R}^N to the original mixed-integer action space of $\mathcal{O}(K^N) \times \mathbb{R}^K$ which is interpretable in the downlink of an OFDMA system. In Section III-C, we use the proximal policy optimization (PPO) [27], [28] algorithm to find optimal actions in \mathbb{R}^N space. Our proposed action space reducer can map the actions taken by the PPO algorithm to the original mixed-integer action space using an optimization framework. Since optimizing the rate allows us to directly control the reliability and latency, we choose the reduced action space to be the rate of each user. However, each user's set of rates will have many corresponding feasible power and RB allocation solutions. We choose the allocation solution with minimum power usage. Hence, we pose a new optimization problem, called *action space reducer*, whose goal is to map the reduced action space which is the rate for each user to the original action space, i.e., RB and power allocation matrices as output so that the power is minimized. This optimization problem maps the action space of our

deep-RL algorithm to the optimization variables in (3). To find this RB and power allocation solution, we formally define the action space reducer problem:

$$\min_{\mathbf{P}, \boldsymbol{\rho}} \sum_{i,j} p_{ij}(t) \quad (9a)$$

$$\text{s.t. } r_i(t) = r_i^d(t), \quad \forall i \in \mathcal{N}, \quad (9b)$$

$$p_{ij}(t) \geq 0, \quad \rho_{ij}(t) \in \{0, 1\}, \quad \forall i \in \mathcal{N}, \quad j \in \mathcal{K}, \quad \forall t, \quad (9c)$$

$$\sum_i \rho_{ij} = 1, \quad \forall j \in \mathcal{K}, \quad (9d)$$

where constraint (9b) guarantees that the rate of each user $r_i(t)$ is set to the desired rate for each user $r_i^d(t)$ while minimizing the total BS power. We can solve (9) with constraint (9b) in the form of an inequality, i.e., $r_i(t) \geq r_i^d(t)$ using an iterative dual decomposition algorithm. As the number of RBs increases, the primal solution converges to the dual solution and the inequality constraint $r_i(t) \geq r_i^d(t)$ will be satisfied in the form of equality [32], [33]. As we will show in Section V, as the number of RBs increases, the error resulting from action space reducer decreases.

The Lagrangian for problem (9) with inequality constraint $r_i(t) \geq r_i^d(t)$ can be written as:

$$L(\mathbf{P}, \boldsymbol{\rho}, \boldsymbol{\lambda}) = \sum_{i,j} p_{ij}(t) - \sum_i \lambda_i (r_i(t) - r_i^d(t)), \quad (10)$$

where $\boldsymbol{\lambda} = [\lambda_1 \quad \lambda_2 \quad \dots \quad \lambda_N]^T$, and:

$$r_i(t) = B \sum_{j=1}^K \log_2 \left(1 + \frac{p_{ij}(t) h_{ij}(t)}{\sigma^2} \right). \quad (11)$$

The dual problem for (9) is:

$$\min_{\mathbf{P}, \boldsymbol{\rho}} L(\mathbf{P}, \boldsymbol{\rho}, \boldsymbol{\lambda}). \quad (12)$$

We can see that the dual problem is decomposable for each RB, i.e., we can write (12) as:

$$\min_{p_{ij}(t)} \sum_i p_{ij}(t) - B \sum_i \lambda_i \log_2 \left(1 + \frac{p_{ij}(t) h_{ij}(t)}{\sigma^2} \right), \quad \forall j \in \mathcal{K}. \quad (13)$$

Each subproblem (13) is convex and has a closed-form solution. By taking the derivative with respect to $p_{ij}(t)$, we have:

$$1 - \lambda_i B \frac{h_{ij}(t)}{(\sigma^2 + p_{ij}^* h_{ij}(t)) \log 2} = 0, \quad \forall i \in \mathcal{N} \quad (14)$$

Hence, for each j we have:

$$p_{ij}^* = \left[\frac{\lambda_i B}{\log 2} - \frac{\sigma^2}{h_{ij}(t)} \right]^+, \quad \forall i \in \mathcal{N}, \quad (15)$$

where $[\cdot]^+$ is equivalent to $\max\{\cdot, 0\}$. Since each RB can be allocated only to one user, we choose to allocate RB j to user i_j where:

$$i_j = \arg \min_i p_{ij}^* - B\lambda_i \log_2 \left(1 + \frac{p_{ij}^* h_{ij}(t)}{\sigma^2} \right), \quad \forall j \in \mathcal{K}. \quad (16)$$

Therefore, we find the RB allocated to each user using (16) and the per-RB power using (15). The only parameter that remains to be determined is λ , which can be derived using the ellipsoid method [32]. After reducing the size of action space, each action becomes $\mathbf{a}_t = [r_1^d(t) \ \dots \ r_N^d(t)] \in \mathbb{R}^N$. The action space then becomes a N -dimensional hyper-cube in \mathbb{R}^N . This space is not still scalable if used with discretization methods (such as the one in [6]). However, since the reduced action space is in \mathbb{R}^N , instead of discretizing, we can find a solution to our deep-RL problem using PPO, as shown next.

C. Optimal Rate Allocation with Policy Gradient

After reducing the action space to \mathbb{R}^N , policy gradient algorithms can effectively control such problems. Among the policy gradient algorithms, we choose PPO, because it has been successfully deployed to cope with high-dimensional continuous action spaces in robotic problems [28]. PPO uses a DNN for mapping the state space into an action space and hence is fast in decision making. A policy gradient algorithm such as PPO can determine $r_i^d(t)$. This is due to the fact that the reduced action space is continuous and using that, we can estimate the gradient of the expected reward of the policy [27]. A policy is a conditional distribution function $\pi_\psi(\mathbf{a}_t|\mathbf{s}_t)$ over a set of actions \mathcal{A} , parametrized by ψ that maps each state \mathbf{s}_t of the system to a distribution. The PPO algorithm tries to indirectly solve the following optimization problem:

$$\max_{\psi} \quad \hat{\mathbb{E}}_t \left\{ \frac{\pi_\psi(\mathbf{a}_t|\mathbf{s}_t)}{\pi_{\psi_{\text{old}}}(\mathbf{a}_t|\mathbf{s}_t)} \hat{A}_t \right\}, \quad (17a)$$

$$\text{s.t.} \quad \text{KL} \{ \pi_\psi(\cdot|\mathbf{s}_t), \pi_{\psi_{\text{old}}}(\cdot|\mathbf{s}_t) \} \leq \delta, \quad (17b)$$

where $\text{KL}\{\cdot\}$ and $\hat{\mathbb{E}}_t$ denote the Kullback-Leibler divergence and an empirical average over a finite batch of samples, respectively. $\pi_\psi(\mathbf{a}_t|\mathbf{s}_t)$ is a stochastic policy, and \hat{A}_t is an estimator of the so-called ‘‘advantage function’’ at time t . The advantage function is a function that captures the relative value of current action in the current state (see [34]). The PPO algorithm transforms optimization problem (17) into following unconstrained optimization objective:

$$\max_{\psi} \quad \hat{\mathbb{E}}_t \left\{ \min \left(\frac{\pi_\psi(\mathbf{a}_t|\mathbf{s}_t)}{\pi_{\psi_{\text{old}}}(\mathbf{a}_t|\mathbf{s}_t)} \hat{A}_t, \text{clip} \left(\frac{\pi_\psi(\mathbf{a}_t|\mathbf{s}_t)}{\pi_{\psi_{\text{old}}}(\mathbf{a}_t|\mathbf{s}_t)}, 1 + \epsilon, 1 - \epsilon \right) \hat{A}_t \right) \right\}, \quad (18)$$

where $\text{clip}\left(\frac{\pi_{\psi}(\mathbf{a}_t|\mathbf{s}_t)}{\pi_{\psi_{\text{old}}}(\mathbf{a}_t|\mathbf{s}_t)}, 1 - \epsilon, 1 + \epsilon\right)$ is a clip function defined as:

$$\text{clip}\left(\frac{\pi_{\psi}(\mathbf{a}_t|\mathbf{s}_t)}{\pi_{\psi_{\text{old}}}(\mathbf{a}_t|\mathbf{s}_t)}, 1 - \epsilon, 1 + \epsilon\right) = \begin{cases} 1 - \epsilon, & \frac{\pi_{\psi}(\mathbf{a}_t|\mathbf{s}_t)}{\pi_{\psi_{\text{old}}}(\mathbf{a}_t|\mathbf{s}_t)} < 1 - \epsilon, \\ \frac{\pi_{\psi}(\mathbf{a}_t|\mathbf{s}_t)}{\pi_{\psi_{\text{old}}}(\mathbf{a}_t|\mathbf{s}_t)}, & 1 - \epsilon \leq \frac{\pi_{\psi}(\mathbf{a}_t|\mathbf{s}_t)}{\pi_{\psi_{\text{old}}}(\mathbf{a}_t|\mathbf{s}_t)} \leq 1 + \epsilon, \\ 1 + \epsilon, & 1 + \epsilon < \frac{\pi_{\psi}(\mathbf{a}_t|\mathbf{s}_t)}{\pi_{\psi_{\text{old}}}(\mathbf{a}_t|\mathbf{s}_t)}. \end{cases} \quad (19)$$

The clip function ensures that the new policy does not diverge from the old policy hence decreasing the variance for learning. We use the gradient of (18) to update our policy $\pi_{\psi}(\mathbf{a}_t|\mathbf{s}_t)$, i.e., find a ψ that maximizes (18). We use a DNN (with weights ψ) to model the policy function $\pi_{\psi}(\mathbf{a}_t|\mathbf{s}_t)$. Then, we find ψ using the PPO algorithm [27], [28]. Ultimately, we obtain an optimal policy $\mu_{\psi^*}(\mathbf{s}_t)$, which at any given state \mathbf{s}_t , provides us with the optimal distribution of actions, i.e., $r_i^d(t)$ for each user $i \in \mathcal{N}$. This action \mathbf{a}_t is mapped to the RB and power allocation matrices using the action space reducer, and hence, this solves our problem.

Now, owing to the PPO and action space reducer, the designed framework can allocate RB and power using a low-complexity and scalable solution. While the developed deep-RL framework can be readily deployed for URLLC, it still needs to be trained in an online manner. Although online training can be done effectively, it can also incur unnecessary overhead as well as long recovery time in case of extreme events. For instance, in case of a sudden rise in arrival rate of all users, the deep-RL system needs a transient time to learn the situation online, i.e., recover and allocate resources efficiently. However, in the URLLC scenarios, this transient time can be crucial to the performance of the system. To overcome this issue, next, we propose the use of GAN to provide our deep-RL agent with experience in a virtual environment so that it is prepared for the extreme cases encountered by a network of URLLC users.

IV. EXPERIENCED DEEP-RL WITH GAN

We now propose a generative method to create a virtual environment for training our deep-RL agent and making it experienced. In particular, we introduce a GAN-based refiner to create a virtual environment that faithfully mimicks a real URLLC environment. This idea is analogous to the recent seminal work by Apple [35] in which the authors used GAN to improve the realism of generating synthetic eye gestures. Inspired by [35], the proposed GAN will use two inputs: a) A limited set of unlabeled real traffic and channel data and b) Synthetic, simulated data generated based on any standard model for the channel and traffic arrival. Using these two inputs, the proposed GAN-based refiner will create a large and realistic dataset that virtually emulates a realistic wireless environment. In other word, the refined, GAN-generated synthetic channel and

traffic data will no longer be distinguishable from real data. Hence, supplementing our real data input with model-based data allows our GAN-based refiner to control the generation of the real-like data. For instance, we can control how fast packets will arrive in the system. *Hence, although the generated data will be similar to real data, we can control it similar to synthetic data.* Using this flexibility in generating real-like data, we can create a virtual environment which is similar to a real URLLC environment. Then, the deep-RL agent can be deployed in this virtual environment to gain experience before being deployed. By doing so, we can reproduce extreme network conditions and use them to better train our deep-RL agent and provide it with experience on a large-scale, diverse set of network conditions. Here, our deep-RL agent will still operate in a model-free fashion.

Fig. 4 shows the analogy between the proposed channel and packet information refiner and the proposed image refiner in [35]. The advantage of our proposed refiner over using completely synthetic information is that it removes the bias in the synthetic information thus making the generated channel distribution, packet length distribution, and packet arrival distribution completely identical to a realistic wireless environment. Moreover, acquiring real datasets on wireless environments is costly, can incur significant overhead on a wireless network, and can raise privacy concerns. Indeed, to date, such real-world datasets remain scarcely available and limited in size. In contrast, using the proposed refiner, without raising any privacy concerns, the network can generate an unlimited set of realistic data at little to no cost and, thus, it will be able to control how many extreme events are in the data. This idea has not been explored in any prior works [6], [18]–[21], [23], [25]–[28], and [35]. Although our work is inspired by [35], in this work, we control the number of extreme events in the dataset which is not studied in [35]. Moreover, the approach in [35] is limited to standard image classification tasks and does not leverage GAN for deep-RL enhancement. Finally, we will analytically derive a bound for controlling similarity of the refined data to the input data, a new result that is not done in [35].

As we previously mentioned, although our deep-RL agent does not need training and can learn while being deployed, using this training process, the agents become suitable for use in URLLC. However, if this environment does not resemble the real URLLC environment, then the deep-RL agent cannot perform well in a realistic environment. This is due to the fact that deep-RL agent needs a transient period to adapt to any new environment. *Hence, we will use the proposed GAN-based refiner to train our deep-RL agent and turn it into an “experienced deep-RL agent” before deployment.* To show how the proposed GAN-assisted, experienced deep-

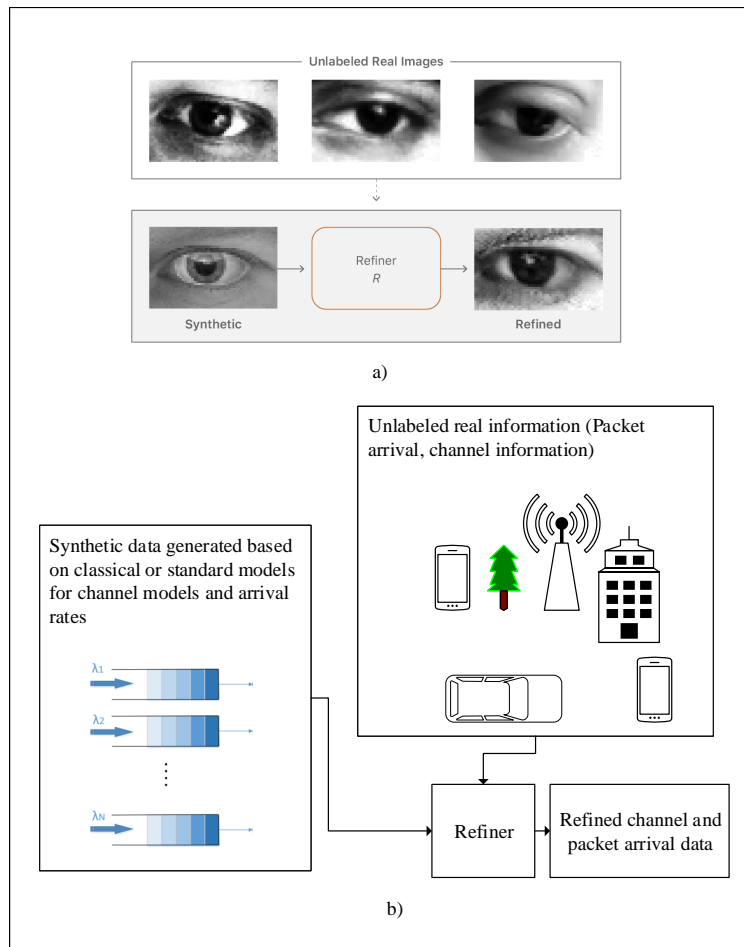


Figure 4: a) Proposed image refiner in [35]. b) Proposed channel and packet information refiner.

RL agent performs, we compare a vanilla deep-RL agent with our experienced deep-RL agent in a wireless environment (having 20 users) in Fig. 5. This figure shows how deploying one experienced agent which has been trained in a virtual environment compares to another agent which has not have any training. As we can see, the trained agent in the virtual environment is able to learn faster and has a shorter transition period. Meanwhile, the untrained agent has a longer transient period during which it does not act optimally. Since URLLC applications are sensitive to reliability and delay, a short period of unreliability or high delay can have a severe effect on a URLLC user. Indeed, this nonoptimal transient period makes the use of an untrained agent (e.g., as done in existing papers on RL for wireless [6], [18]–[21]) ill-suited for adoption in mission critical URLLC applications. Hence, by designing a GAN-based virtual environment, our goal is to eliminate this transient period when the deep-RL agent is deployed in an actual wireless network. To the best of our knowledge, no prior work investigated the effect of these

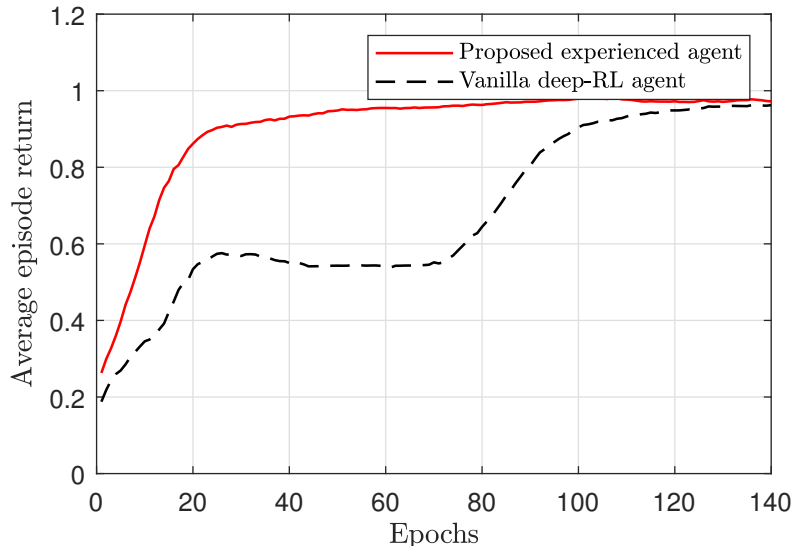


Figure 5: Deploying an untrained and an experienced agent in a URLLC environment.

transient periods when using deep-RL for wireless networking.

Designing a virtual wireless environment faces some challenges. If this virtual environment is entirely synthetic, then the transient training period will not be removed. This is due to the fact that even slight changes compared to a real environment cause the deep-RL agent not to make decision optimally. On the other hand, if this virtual environment is entirely based on collected real wireless data, it does not include enough extreme events. Therefore, this gathered real data does not cover all the unexpected situations for the deep-RL agent. This requires the deep-RL agent to go through a training period when it encounters an extreme event in the URLLC system. As we observe from Fig. 5, this training period from epoch 20 to epoch 100 can cause a failure in the URLLC system. Furthermore, gathering real data for a real URLLC environment is very time consuming and expensive. Hence our designed refiner has two goals: 1) The output of the refiner (packet length, interarrival times, channel gains) must be indistinguishable from a real dataset, i.e., it is from the same distribution as the real dataset and 2) The output of the refiner must have some form of similarity to the input of the refiner. This makes the refiner preserve the main characteristics of the synthetic dataset, e.g., short interarrival time or large packets.

To make the output of the refiner indistinguishable from a real dataset, we use a discriminator neural network along with our refiner neural network [36]. We assume that the refiner neural network is trained as follows:

$$\theta_R^* = \arg \min_{\theta_R} \max_{\theta_D} f(\theta_R, \theta_D) = \arg \min_{\theta_R} f(\theta_R, \theta_D^*(\theta_R)), \quad (20a)$$

$$\text{s.t. } \mathbb{E}_{z \sim g_{\text{sim}}} [\|F(z; \theta_R) - z\|] < \epsilon_r, \quad (20b)$$

where θ_R is the set of weights for the refiner neural network, which is the network that gets synthetic data z as input and generates refined real-like data $F(z; \theta_R)$ as output. In our problem, z is equivalent to synthetic state variables s_t that we generate for training our deep-RL algorithm. θ_D is the set of weights of the discriminator, the network that discriminates between the refined data $F(z; \theta_R)$ and real data. θ_D^* is the optimal set of weights for the discriminator, i.e., the trained discriminator network that can find out if the data is real or not. g_{sim} is the distribution of synthetic data, e.g., Rayleigh distribution or Poisson packet length distribution. z is a sample from the distribution g_{sim} and $F(z; \theta_R)$ is output of the refiner network. By optimizing the objective in (20a), we make sure that the distribution of the real data and generated data are the same. Moreover, (20b) guarantees the similarity of input of the refiner z and the output of the refiner $F(z; \theta_R)$. If we increase ϵ_r in (20b), we can allow the output of the refiner to differ more from the synthetic dataset and be indistinguishable from the real dataset. On the other hand, if we decrease ϵ_r , we limit the output of the refiner network to be similar to its input which is the synthetic data. However, if ϵ_r is less than a certain value, then the optimization problem (20) becomes infeasible because the refined samples which are noticeably similar to the synthetic dataset are easily identifiable by the discriminator. Next, in Theorem 2, we rigorously set a insightful guideline for choosing ϵ_r so that the problem (20) becomes feasible and also becomes responsive to the input of the refiner (synthetic data).

Theorem 2. The optimization problem (20) is not feasible if $\epsilon_r < \epsilon_r^t$, where:

$$\epsilon_r^t = \sqrt{\|\mu_R\|^2 + \|\mu_z\|^2 - 2\mu_R^T \mu_z}. \quad (21)$$

μ_R and μ_z are the expectations of $F(z; \theta_R^*)$ and z , respectively, i.e., $\mu_R = \mathbb{E}_{z \sim g_{\text{sim}}} [F(z; \theta_R^*)]$ and $\mu_z = \mathbb{E}_{z \sim g_{\text{sim}}} [z]$.

Proof: See Appendix A. ■

Theorem 2 provides guidelines for choosing the value of ϵ_r . ϵ_r must be within a certain range so that the output of the refiner is meaningful. Since refiner is a neural network, it is a flexible function. Hence, if we keep the value of ϵ_r close to the ϵ_r^t it will still generate outputs which are entirely similar to the input, and do not have the properties of the real data. Similarly, we can see that by significantly increasing the value of ϵ_r , we will have no control over the output of the refiner, and the output becomes thoroughly similar to the real data. The constrained refiner

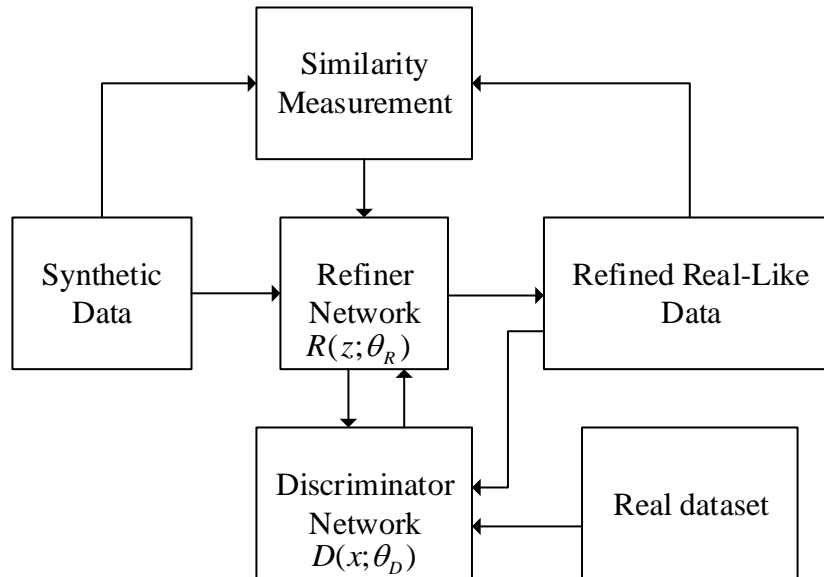


Figure 6: Proposed model for GAN based refiner.

optimization problem can be transformed using Lagrange multiplier to:

$$\theta_R^* = \arg \min_{\theta_R} \max_{\theta_D} f(\theta_R, \theta_D) = \arg \min_{\theta_R} f(\theta_R, \theta_D^*(\theta_R)) + \lambda_r \mathbb{E}_{z \sim g_{\text{sim}}} [\|F(z; \theta_R) - z\|] \quad (22)$$

$$\theta_D^*(\theta_R) = \arg \max_{\theta_D} f(\theta_R, \theta_D), \quad (23)$$

where f is a cross entropy loss defined to be:

$$f(\theta_R, \theta_D) = \mathbb{E}_{x \sim p_{\text{env}}} [\log(D(x; \theta_D))] + \mathbb{E}_{z \sim g_{\text{sim}}} [\log(1 - D(F(z; \theta_R); \theta_D))], \quad (24)$$

where p_{env} is the distribution of real dataset (real wireless environment) and $D(x; \theta_D)$ is the output of discriminator neural network parametrized by θ_D when the input x is given. The term $f(\theta_R, \theta_D^*(\theta_R))$ in (22) is the objective function of the generative refiner which is minimizing the average correct predictions by the discriminator network D . This objective function defined in (24) is high when the discriminator D is able to discriminate between the real data distributed according to p_{env} and refined simulated data distributed according to g_{sim} . Also, the term $\mathbb{E}_{z \sim g_{\text{sim}}} [\log(1 - D(F(z; \theta_R); \theta_D))]$ in (22) guarantees that the output of the refiner is similar to the input of the refiner. λ_r in (22) balances the similarity between the input and the output of the refiner and similarity to the real dataset. We can see from Fig. 6 that the refiner tries to reach its two mentioned goals while the discriminator tries to discriminate the real data from the refined synthetic data. The similarity between the input and output of the refiner helps to control the level of extreme events in the generated dataset.

V. SIMULATION RESULTS AND ANALYSIS

We simulate a square area of size $500\text{ m} \times 500\text{ m}$ in which 20 users are served by an OFDMA system with a total bandwidth of 45 MHz, an RB bandwidth of $B = 180\text{ kHz}$, and a noise power spectral density $N_0 = -173.9\frac{\text{dBm}}{\text{Hz}}$, (unless stated otherwise). We set the path loss exponent to 3 (urban area) and the carrier frequency to 2 GHz. We set the maximum BS power to 4 W and each user's latency D_i^{\max} to 10 ms, unless stated otherwise. For the packet arrival and packet sizes, we used the dataset of [37]. Since each row in the dataset was for a session, we could not access each individual packet size, and interarrival time (IAT). Hence, for each session, we generated the total number of packets with the mean size and IAT mean mentioned in the dataset in [37]. For evaluation, we assume that the packets arriving from the dataset are similar in length and IAT for all users. However, the proposed deep-RL framework will be model-free and does not have any information about this traffic model.

A. Experienced Deep-RL Results

Fig. 7 shows the effect of training an experienced deep-RL agent in the proposed GAN-generated virtual environment, for a network with 10 users. In this experiment, two agents are deployed in a wireless environment in which packets and IAT are generated based on the dataset in [37]. We created a virtual environment for training. This virtual environment is a refined version of an M/M/1 arrival with an average packet length of 300 bytes and IAT of 250 microseconds. We considered these packet length and IAT as an extreme condition because this IAT is smaller than 25% of all packets' IAT in the real dataset, and this packet length is larger than 75% of all packets' length in the real dataset. Our experienced deep-RL agent is trained beforehand in the described virtual environment. The other agent does not have any training, and its neural networks are initialized randomly. During the deployment of these two agents, at epoch 50, we change the environment to an extreme environment. This extreme environment has a large packet length and smaller IAT. As we can see from Fig. 7, the trained agent can recover around 50 epochs faster than the untrained agent. This shows that the virtual environment created using the proposed GAN-refiner can make the trained agent ready for real extreme events, and makes the system resilient to such unpredictable extreme events. This resiliency is an inherent part of URLLC, and it is especially important for mission-critical applications. A short period of unreliability or long delays can cause irreversible damages to such applications.

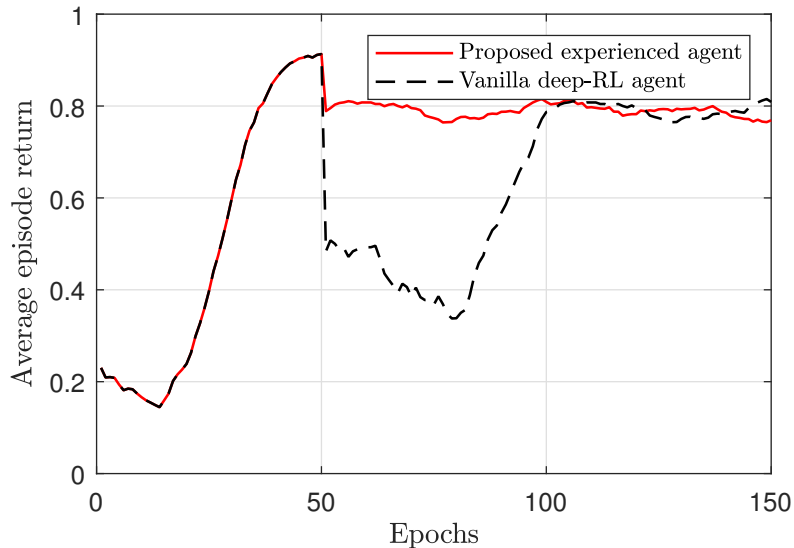


Figure 7: Effect of training a deep-RL agent in the proposed GAN-generated virtual environment.

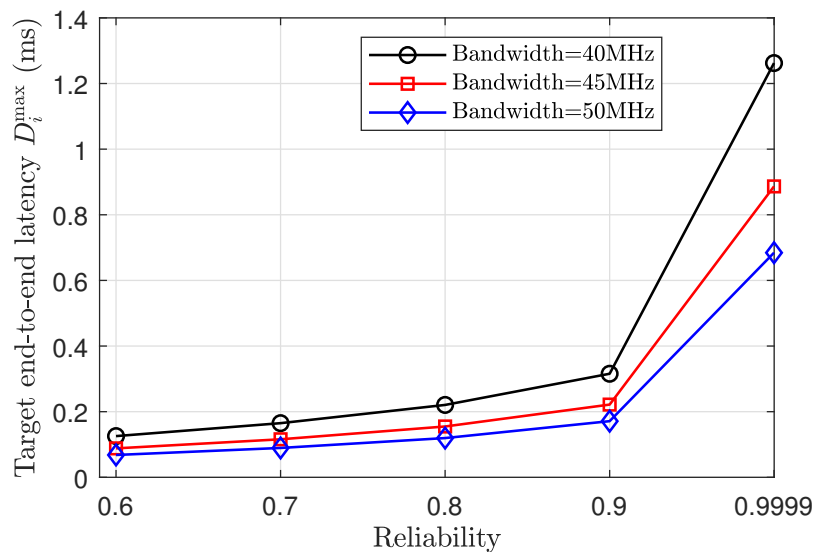


Figure 8: Effect of bandwidth on delay-reliability tradeoff for the proposed system.

Fig. 8 shows the effect of the maximum bandwidth on the delay-reliability tradeoff. Here, we use the target latency D_i^{\max} because it is the threshold for our reliability analysis. We can see that, as we allocate more bandwidth to the system, we are able to achieve higher reliability and lower latency with the same rate. For instance, by increasing the bandwidth from 45 MHz to 50 MHz, we are able to decrease the latency of each user by 16%. Also we can see that increasing the target latency increases the reliability in the system. This is because larger target latencies makes it easier for the system to satisfy the associated (looser) reliability requirements.

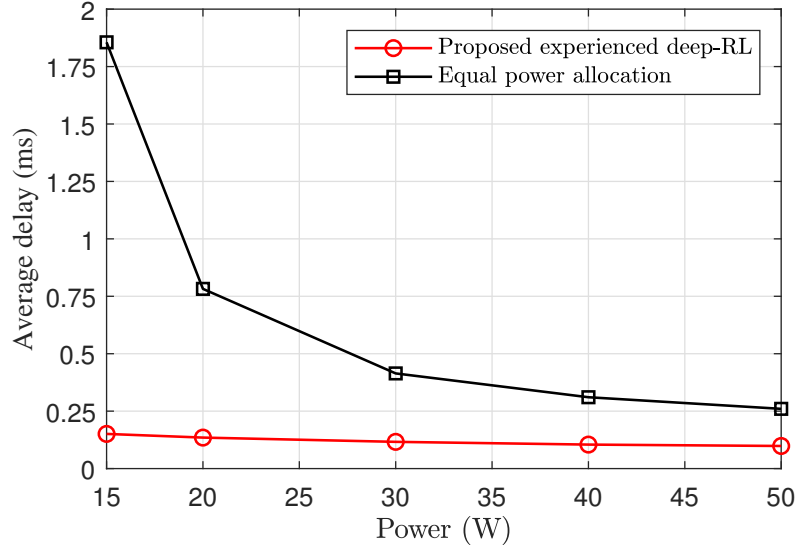


Figure 9: Effect of BS power on the average delay of the system.

We can also see that the reliability of 99.99% and latency of less than 1.5 ms is achievable in our system.

Fig. 9 shows the effect of the BS power on the average delay of the system. For performance assessment, we have used a heuristic algorithm to compare the performance with the proposed experienced deep-RL agent. In this heuristic, which we refer to as equal power allocation, we divide the power equally for each RB. Then, we assign each RB to the user with highest channel gain on that RB. Fig. 9 shows that our proposed method outperforms the heuristic method, particularly, at lower power regimes. This is because the impact of the optimal channel and power allocation is more pronounced when the resource is scarce. In this regard, our proposed approach achieves a gain of at least 62% (at 15 W) and up to 91%, compared to the baseline. Moreover, our system can reach average delays as low as 0.15 milliseconds (for small packet sizes) which is suitable for many ultra low latency systems. Such a threshold is not achieved by the baseline.

B. Deep-RL algorithm

Next, we provide a set of simulations in which we use only synthetic data in order to showcase the performance of our proposed deep-RL algorithm over a broad range of parameters which are not available within the existing, limited real datasets.

Fig. 10 shows the relation between the arrival rate (i.e., minimum required data rate for a user), maximum delay, and reliability in our system. As we mentioned, the rate, reliability, and

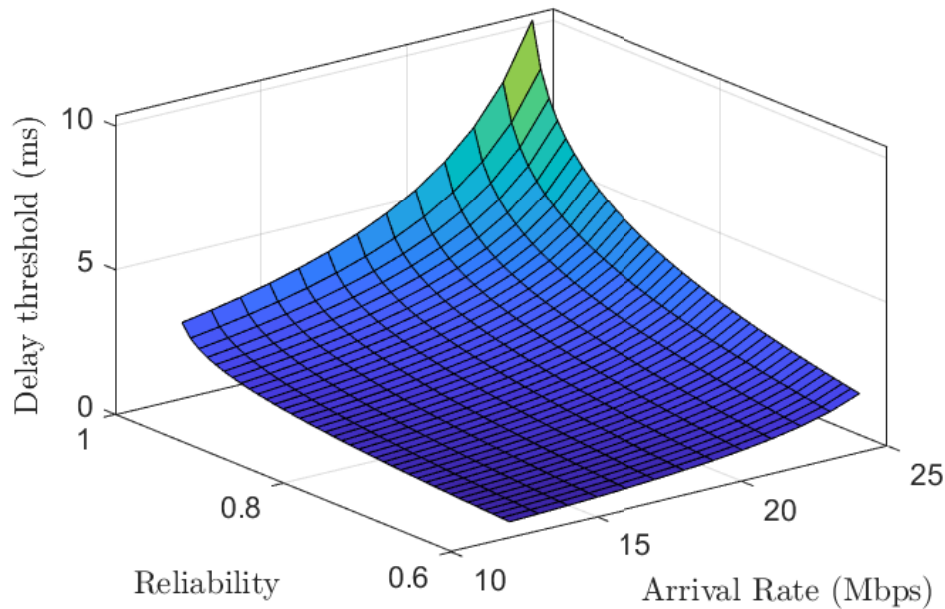


Figure 10: 3D plot of the achievable arrival rate, delay, and reliability for the system.

latency are incompatible design parameters. However, since our system can attain any feasible combination of the rate, reliability, and latency, we can enable URLLC with reliability of 99% and latency of 4.2 ms with the rate of 1 Mbps, and a reliable high-rate communication with 99% reliability and rate of 10 Mbps with latency of 24.5 ms at the same time. Also, the system can balance between rate, reliability, and latency. As an example, we can see from Fig. 10 that, our system is able to provide ultra-reliable low latency communication with a delay of 8 milliseconds and a reliability of 98% with a rate of 7 Mbps. However, if we need higher rate for this system, without decreasing reliability or increasing latency, then we have to allocate a higher bandwidth to the system. We can increase the rate of each one of the 20 user to 46 Mbps if we increase the system bandwidth from 45 MHz to 200 MHz and the power from 5 W to 20 W. These results provide insightful guidelines for controlling the rate-reliability-delay tradeoff. For example, we see that with a reliability of 98%, delay of 8 ms, and rate of 7 Mbps, a gain of 1% reliability can be done with 47% less delay but at the expense of a seven-fold decrease in the rate.

The effect of packet size on the reliability of the system with $D_i^{\max} = 10$ ms is shown in Fig. 11. We can see that, for higher rates, the effect of packet size becomes more dominant. The system can only provide more reliability to the traffic with shorter packet sizes. This is due to the fact that applications with shorter packets naturally have a smaller end-to-end delay. Hence, it is less challenging for our system to provide ultra high reliability to such applications. Fig. 11

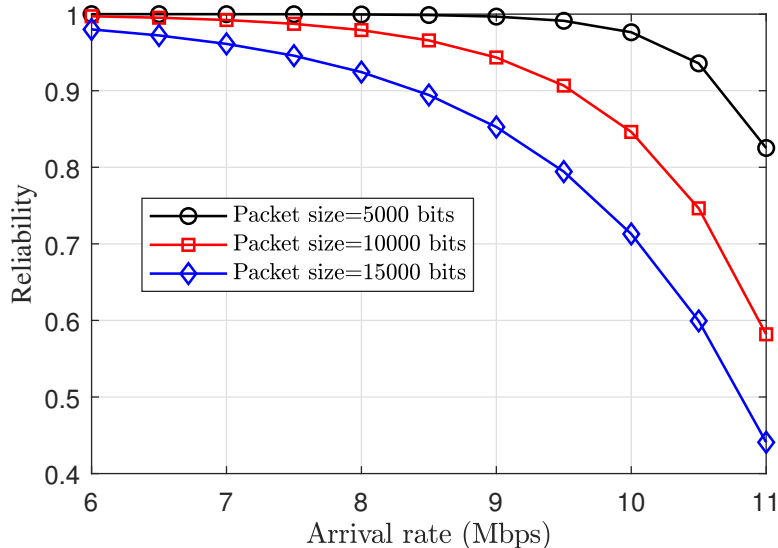


Figure 11: Effect of packet size on rate-reliability tradeoff for the designed system.

shows that our system is able to reach URLLC reliability and latency as well as higher data rates with moderate latency and reliability for high data rate and large packet size applications. We can see that at higher data rates the reliability decreases, and this is because the limited bandwidth and power in the system can guarantee reliability up to a certain rate. We can increase this reliable rate by either decreasing packet size, increasing bandwidth, increasing power, and/or increasing target end-to-end latency.

Fig. 12 shows the per user error of the action reducer defined as $E = \frac{\|\mathbf{r} - \mathbf{r}^d\|}{N\|\mathbf{r}\|}$, where \mathbf{r} is the vector of wireless downlink downlink rate and \mathbf{r}^d is the vector of desired rate. This error measures the distance between the input and output rate of action space reducer. We can see that, as the bandwidth of each RB decreases, the number of RBs increases in the system, and hence, the error of our action space reducer will decrease. We can see that, for an RB bandwidth of 180 kHz (typical for LTE), the error is less than 1% for each user.

VI. CONCLUSION

In this paper, we have proposed a novel *experienced* deep-RL framework to provide model-free URLLC in the downlink of an OFDMA system. Our proposed deep-RL framework can guarantee high end-to-end reliability and low end-to-end latency, under explicit data rate constraints without any models or assumptions on the users' traffic. In particular, to enable the deep-RL framework to account for extreme network conditions and operate in highly reliable systems, we have

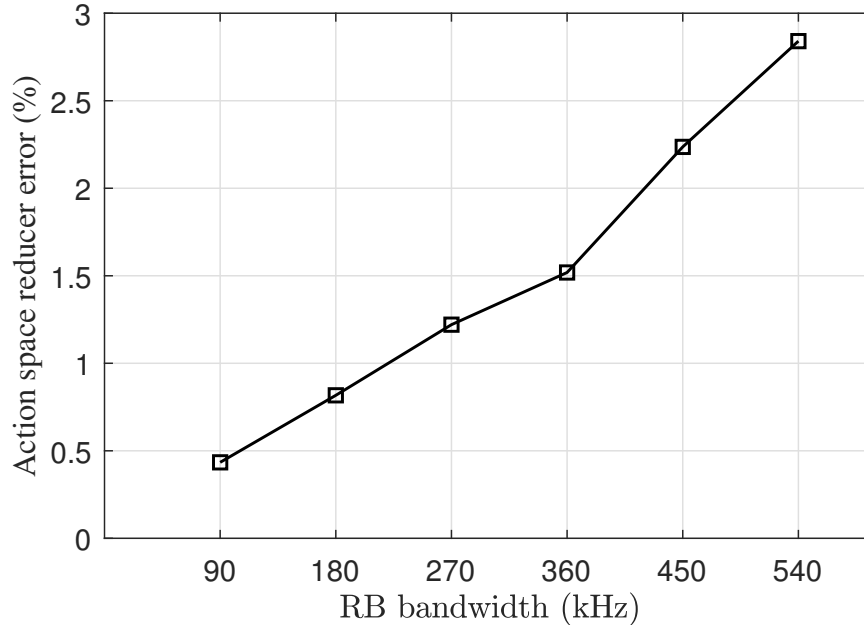


Figure 12: Effect of resource block bandwidth on the per user error of the action reducer.

proposed a new approach based on GANs, namely, GAN-based refiner. We have used this GAN-based refiner to pre-train the deep-RL agent utilizing a mix of real and synthetic data. Using this GAN-based refiner, we can expose our deep-RL agent to a broad range of network conditions. We have also shown that our proposed approach can predict the users' traffic using the experienced deep-RL framework and subsequently use those predictions in the resource allocation process. We have formulated the problem as a power minimization problem under reliability, latency, and rate constraints. To solve this problem, first, we have determined the rate of each user using experienced deep-RL. Then, using a proposed action space reducer, we have mapped these rates to the resource block and power allocation vectors of a wireless system. Finally, we have used the end-to-end reliability and latency of each user as feedback to the deep-RL framework. We have demonstrated that, at the fixed-point of the deep-RL algorithm, the reliability and latency of the users are guaranteed. Moreover, we have derived some analytical bounds for the output of the proposed GAN-based refiner. Our results have shown that the proposed approach can achieve the required performance in the rate-reliability-latency region. Also, we have demonstrated that the proposed experienced deep-RL framework is suitable for URLLC applications because it can: a) remove the transient training time that exists in conventional deep-RL methods and b) recover faster in the case of unexpected extreme events which cause failure in URLLC systems. The proposed experienced deep-RL framework can also be adopted in many future wireless

applications that require adaptive and quick optimization algorithms.

APPENDIX A

PROOF OF THEOREM 2

Proof: Assuming the cross entropy loss function, we have:

$$\begin{aligned}
f(\theta_R, \theta_D) &= \mathbb{E}_{x \sim p_{\text{env}}} [\log(D(x; \theta_D))] + \mathbb{E}_{z \sim g_{\text{sim}}} [\log(1 - D(F(z; \theta_R); \theta_D))] \\
&= \int_x [\log(D(x; \theta_D))] p_{\text{env}}(x) dx + \int_z [\log(1 - D(F(z; \theta_R); \theta_D))] g_{\text{sim}}(z) dz \\
&= \int_x [\log(D(x; \theta_D))] p_{\text{env}}(x) + [\log(1 - D(x; \theta_D))] p_r(x) dx, \tag{25}
\end{aligned}$$

where $p_r(x)$ is distribution of the refiner outputs. We know that for all the functions c in the form of $c(v) = a \log(v) + b \log(1 - v)$ and any $(a, b) \in \mathbb{R}^2 \setminus \{0, 0\}$, the maximum in the set $v \in [0, 1]$ is at $v = \frac{a}{a+b}$. Hence, we know that

$$\begin{aligned}
\max_{\theta_D} f(\theta_R, \theta_D) &= \int_x [\log(\frac{p_{\text{env}}(x)}{p_{\text{env}}(x) + p_r(x)})] p_{\text{env}}(x) + [\log(1 - \frac{p_{\text{env}}(x)}{p_{\text{env}}(x) + p_r(x)})] p_r(x) dx \\
&= \text{KL}(p_{\text{env}} \| p_{\text{env}}(x) + p_r(x)) + \text{KL}(p_r(x) \| p_{\text{env}}(x) + p_r(x)), \tag{26}
\end{aligned}$$

We know that right hand side of (26) is minimized when $p_{\text{env}}(x) = p_r(x)$. However, since (20) is a constrained optimization problem we should consider conditions other than optimality to find its optimum. Considering the complementary slackness condition in the Karush-Kuhn-Tucker (KKT) conditions for (20), we know that the final solution, at least one of following two conditions should be satisfied. 1) The final solution of (20a) should satisfy the (20b), i.e.,

$$\mathbb{E}_{z \sim g_{\text{sim}}} [\|F(z; \theta_R^*) - z\|] = \epsilon_r, \tag{27}$$

or 2) the optimal solution is same as the solution of unconstrained version of (20) which is $p_{\text{env}}(x) = p_r(x)$.

In case 2) when $\epsilon_r \rightarrow \infty$, the problem becomes unconstrained optimization and the refiner works as if its only goal is to generate more realistic samples instead of controlling the outputs of the refiner. However, in case 1) we have:

$$\begin{aligned}
\mathbb{E}_{z \sim g_{\text{sim}}} [\|F(z; \theta_R^*) - z\|^2] &= \mathbb{E}_{z \sim g_{\text{sim}}} [(F(z; \theta_R^*) - z)^T (F(z; \theta_R^*) - z)] \\
&= \text{tr}(\mathbb{E}_{z \sim g_{\text{sim}}} [(F(z; \theta_R^*) - z)^T (F(z; \theta_R^*) - z)]) \\
&= \mathbb{E}_{z \sim g_{\text{sim}}} [\text{tr}((F(z; \theta_R^*) - z)^T (F(z; \theta_R^*) - z))] \\
&= \mathbb{E}_{z \sim g_{\text{sim}}} [\text{tr}((F(z; \theta_R^*) - z)(F(z; \theta_R^*) - z)^T)] \\
&= \mathbb{E}_{z \sim g_{\text{sim}}} [\text{tr}(F(z; \theta_R^*) F(z; \theta_R^*)^T + z z^T - 2F(z; \theta_R^*) z^T)]
\end{aligned}$$

$$\begin{aligned}
&= \text{tr}(\mathbb{E}_{z \sim g_{\text{sim}}} [F(z; \theta_R^*) F(z; \theta_R^*)^T]) + \text{tr}(\mathbb{E}_{z \sim g_{\text{sim}}} [z z^T]) \\
&\quad - 2\text{tr}(\mathbb{E}_{z \sim g_{\text{sim}}} [F(z; \theta_R^*) z^T]) \\
&= \text{tr}(\text{VAR}(F(z; \theta_R^*)) + \mu_R \mu_R^T) + \text{tr}(\text{VAR}(z) + \mu_z \mu_z^T) \\
&\quad - 2\text{tr}(\text{COV}[z; \theta_R^*] z) + \mu_z \mu_R^T \\
&= \text{tr}(\text{VAR}(F(z; \theta_R^*))) + \text{tr}(\text{VAR}(z)) - 2\text{tr}(\text{COV}(z, F(z; \theta_R^*))) \\
&\quad + \text{tr}(\mu_R^T \mu_R) + \text{tr}(\mu_z^T \mu_z) - 2\text{tr}(\mu_R^T \mu_z) \\
&= \text{tr}(\text{VAR}(F(z; \theta_R^*))) + \text{tr}(\text{VAR}(z)) - 2\text{tr}(\text{COV}(z, F(z; \theta_R^*))) \\
&\quad + \|\mu_R\|^2 + \|\mu_z\|^2 - 2\mu_R^T \mu_z, \tag{28}
\end{aligned}$$

where $\text{tr}(\cdot)$ is the trace of a matrix, μ_R and μ_z are the expectations of $F(z; \theta_R^*)$ and z , respectively, i.e., $\mu_R = \mathbb{E}_{z \sim g_{\text{sim}}} [F(z; \theta_R^*)]$ and $\mu_z = \mathbb{E}_{z \sim g_{\text{sim}}} [z]$. $\text{COV}(\cdot)$ and $\text{VAR}(\cdot)$ are cross-covariance and covariance matrix of random vectors, respectively. The operations in (28) are using the fact that both $\mathbb{E}_{z \sim g_{\text{sim}}}(\cdot)$ and $\text{tr}(\cdot)$ are linear operators and using the properties of function $\text{tr}(\cdot)$. Using the Cauchy-Schwarz inequality, we know that

$$\text{tr}(\text{VAR}(F(z; \theta_R^*))) + \text{tr}(\text{VAR}(z)) - 2\text{tr}(\text{COV}(z, F(z; \theta_R^*))) \geq 0. \tag{29}$$

Inequality (29) is tight when where the random vectors $\text{VAR}(F(z; \theta_R^*))$ and z are completely correlated. Hence, we can see that

$$\mathbb{E}_{z \sim g_{\text{sim}}} [\|F(z; \theta_R^*) - z\|^2] = \epsilon_r^2 \geq \|\mu_R\|^2 + \|\mu_z\|^2 - 2\mu_R^T \mu_z, \tag{30}$$

and hence the minimum value for the ϵ_r is as follows:

$$\epsilon_r \geq \sqrt{\|\mu_R\|^2 + \|\mu_z\|^2 - 2\mu_R^T \mu_z} = \epsilon_r^t. \tag{31}$$

REFERENCES

- [1] A. Taleb Zadeh Kasgari and W. Saad, "Model-Free ultra reliable low latency communication (URLLC): a deep reinforcement learning framework," in *Proc. of IEEE International Conference on Communications (ICC)*, Shanghai, P.R. China, May 2019.
- [2] M. Mozaffari, W. Saad, M. Bennis, and M. Debbah, "Mobile unmanned aerial vehicles (uavs) for energy-efficient internet of things communications," *IEEE Transactions on Wireless Communications*, vol. 16, no. 11, pp. 7574–7589, Nov 2017.
- [3] M. Bennis, M. Debbah, and H. V. Poor, "Ultrareliable and low-latency wireless communication: Tail, risk, and scale," *Proceedings of the IEEE*, vol. 106, no. 10, pp. 1834–1853, Oct 2018.
- [4] W. Saad, M. Bennis, and M. Chen, "A vision of 6G wireless systems: Applications, trends, technologies, and open research problems," *IEEE Network*, 2019.
- [5] I. Parvez, A. Rahmati, I. Guvenc, A. I. Sarwat, and H. Dai, "A survey on low latency towards 5G: RAN, core network and caching solutions," *IEEE Communications Surveys Tutorials*, vol. 20, no. 4, pp. 3098–3130, Fourth Quarter 2018.
- [6] H. Ye and G. Y. Li, "Deep reinforcement learning for resource allocation in V2V communications," in *Proc. of IEEE International Conference on Communications (ICC), Kansas City, MO, USA*. IEEE, July 2018, pp. 1–6.
- [7] A. Ferdowsi, U. Challita, W. Saad, and N. B. Mandayam, "Robust deep reinforcement learning for security and safety in autonomous vehicle systems," in *Proc. of the 21st International Conference on Intelligent Transportation Systems (ITSC)*, Nov 2018, pp. 307–312.
- [8] M. Chen, W. Saad, and C. Yin, "Virtual reality over wireless networks: Quality-of-service model and learning-based resource management," *IEEE Transactions on Communications*, vol. 66, no. 11, pp. 5621–5635, Nov 2018.

- [9] C. Liu and M. Bennis, "Ultra-reliable and low-latency vehicular transmission: An extreme value theory approach," *IEEE Communications Letters*, vol. 22, no. 6, pp. 1292–1295, June 2018.
- [10] Z. Hou, C. She, Y. Li, T. Q. S. Quek, and B. Vucetic, "Burstiness-aware bandwidth reservation for ultra-reliable and low-latency communications in tactile internet," *IEEE Journal on Selected Areas in Communications*, vol. 36, no. 11, pp. 2401–2410, Nov 2018.
- [11] W. K. Lai and C.-L. Tang, "QoS-aware downlink packet scheduling for LTE networks," *Computer Networks*, vol. 57, no. 7, pp. 1689–1698, May 2013.
- [12] Z. Zhou, R. Ratasuk, N. Mangalvedhe, and A. Ghosh, "Resource allocation for uplink grant-free ultra-reliable and low latency communications," in *Proc. of IEEE 87th Vehicular Technology Conference (VTC Spring)*, June 2018, pp. 1–5.
- [13] M. Yousefvand and N. B. Mandayam, "Joint user association and resource allocation optimization for ultra reliable low latency hetnets," *arXiv preprint arXiv:1809.06550*, 2018.
- [14] S. Samarakoon, M. Bennis, W. Saad, and M. Debbah, "Federated learning for ultra-reliable low-latency V2V communications," *arXiv preprint arXiv:1805.09253*, 2018.
- [15] M. I. Ashraf, C. Liu, M. Bennis, W. Saad, and C. S. Hong, "Dynamic resource allocation for optimized latency and reliability in vehicular networks," *IEEE Access*, vol. 6, pp. 63 843–63 858, 2018.
- [16] A. T. Z. Kasgari, W. Saad, and M. Debbah, "Human-in-the-loop wireless communications: Machine learning and brain-aware resource management," *IEEE Transactions on Communications*, To appear, 2019.
- [17] A. Anand, G. D. Veciana, and S. Shakkottai, "Joint scheduling of URLLC and eMBB traffic in 5G wireless networks," in *Proc. IEEE Conference on Computer Communications (INFOCOM)*, April 2018, pp. 1970–1978.
- [18] Y. He, F. R. Yu, N. Zhao, H. Yin, and A. Boukerche, "Deep reinforcement learning (DRL)-based resource management in software-defined and virtualized vehicular Ad Hoc networks," in *Proc. of ACM Symposium on Development and Analysis of Intelligent Vehicular Networks and Applications, Miami, FL, USA*, April 2018, pp. 47–54.
- [19] Z. Xu, Y. Wang, J. Tang, J. Wang, and M. C. Gursoy, "A deep reinforcement learning based framework for power-efficient resource allocation in cloud RANs," in *Proc. of IEEE International Conference on Communications (ICC), Paris, France*, May 2017, pp. 1–6.
- [20] J. Li, H. Gao, T. Lv, and Y. Lu, "Deep reinforcement learning based computation offloading and resource allocation for MEC," in *Proc. IEEE Wireless Communications and Networking Conference, Barcelona, Spain*, April 2018, pp. 1–6.
- [21] K. I. Ahmed, H. Tabassum, and E. Hossain, "Deep learning for radio resource allocation in multi-cell networks," *IEEE Network*, to appear, 2019.
- [22] H. Sun, X. Chen, Q. Shi, M. Hong, X. Fu, and N. D. Sidiropoulos, "Learning to optimize: Training deep neural networks for wireless resource management," in *Proc. of IEEE 18th International Workshop on Signal Processing Advances in Wireless Communications (SPAWC), Sapporo, Japan*, July 2017, pp. 1–6.
- [23] A. Azari, M. Ozger, and C. Cavdar, "Risk-aware resource allocation for URLLC: Challenges and strategies with machine learning," *arXiv preprint arXiv:1901.04292*, 2018.
- [24] M. Chen, M. Mozaffari, W. Saad, C. Yin, M. Debbah, and C. S. Hong, "Caching in the sky: Proactive deployment of cache-enabled unmanned aerial vehicles for optimized quality-of-experience," *IEEE Journal on Selected Areas in Communications*, vol. 35, no. 5, pp. 1046–1061, May 2017.
- [25] V. Mnih, K. Kavukcuoglu, D. Silver, A. A. Rusu, J. Veness, M. G. Bellemare, A. Graves, M. A. Riedmiller, A. Fidjeland, G. Ostrovski, S. Petersen, C. Beattie, A. Sadik, I. Antonoglou, H. King, D. Kumaran, D. Wierstra, S. Legg, and D. Hassabis, "Human-level control through deep reinforcement learning," *Nature*, vol. 518, no. 7540, p. 529, Feb. 2015.
- [26] T. P. Lillicrap, J. J. Hunt, A. Pritzel, N. Heess, T. Erez, Y. Tassa, D. Silver, and D. Wierstra, "Continuous control with deep reinforcement learning," in *Proc. of the International Conference on Learning Representations, ICLR 2016, San Juan, Puerto Rico, May*, 2016.
- [27] J. Schulman, F. Wolski, P. Dhariwal, A. Radford, and O. Klimov, "Proximal policy optimization algorithms," *arXiv preprint arXiv:1707.06347*, 2017.
- [28] N. Heess, S. Sriram, J. Lemmon, J. Merel, G. Wayne, Y. Tassa, T. Erez, Z. Wang, S. Eslami, M. Riedmiller, and D. Silver, "Emergence of locomotion behaviours in rich environments," *arXiv preprint arXiv:1707.02286*, 2017.
- [29] H. Ye, G. Y. Li, B.-H. F. Juang, and K. Sivanesan, "Channel agnostic end-to-end learning based communication systems with conditional gan," *arXiv preprint arXiv:1807.00447*, 2018.
- [30] H. Ye, G. Y. Li, and B.-H. F. Juang, "Deep learning based end-to-end wireless communication systems with conditional gan as unknown channel," *arXiv preprint arXiv:1903.0255*, 2019.
- [31] A. Ferdowsi and W. Saad, "Generative adversarial networks for distributed intrusion detection in the internet of things," in *Proc. of the IEEE Global Communications Conference (GLOBECOM), Waikoloa, HI, USA*. IEEE, December 2019.
- [32] W. Yu and R. Lui, "Dual methods for nonconvex spectrum optimization of multicarrier systems," *IEEE Transactions on Communications*, vol. 54, no. 7, pp. 1310–1322, July 2006.
- [33] A. T. Z. Kasgari and W. Saad, "Stochastic optimization and control framework for 5G network slicing with effective isolation," in *Proc. of 52nd Annual Conference on Information Sciences and Systems (CISS), Princeton, NJ, USA*, March 2018, pp. 1–6.
- [34] R. S. Sutton and A. G. Barto, *Reinforcement learning: An introduction*. MIT press, 2018.
- [35] A. Shrivastava, T. Pfister, O. Tuzel, J. Susskind, W. Wang, and R. Webb, "Learning from simulated and unsupervised images through adversarial training," in *Proc. of IEEE Conference on Computer Vision and Pattern Recognition (CVPR), Honolulu, HI, USA*, July 2017.
- [36] I. Goodfellow, J. Pouget-Abadie, M. Mirza, B. Xu, D. Warde-Farley, S. Ozair, A. Courville, and Y. Bengio, "Generative adversarial nets," in *Proc. of Advances in Neural Information Processing Systems*. Curran Associates, Inc., 2014, pp. 2672–2680.
- [37] J. S. Rojas, Á. R. Gallón, and J. C. Corrales, "Personalized service degradation policies on OTT applications based on the consumption behavior of users," in *Proceedings of Computational Science and Its Applications - ICCSA 2018 - 18th, Melbourne, VIC, Australia, July 2-5, 2018, Part III*, 2018, pp. 543–557.